Available online at www.sciencedirect.com
ScienceDirect
Continental Shelf Research 29 (2009) 136–147
CONTINENTAL SHELF RESEARCH
www.elsevier.com/locate/csr

Initial growth of phytoplankton in turbid estuaries: A simple model

H.E. de Swart[a,*], H.M. Schuttelaars[b], S.A. Talke[a,1]

[a]Institute for Marine and Atmospheric Research (IMAU), Utrecht University, Princetonplein 5, 3584 CC Utrecht, The Netherlands
[b]Applied Mathematical Analysis, Technical University Delft, Mekelweg 4, 2628 CD Delft, The Netherlands

Received 15 January 2007; received in revised form 7 July 2007; accepted 24 September 2007
Available online 4 October 2007

Abstract

An idealised model is presented and analysed to gain more fundamental understanding about the dynamics of phytoplankton blooms in well-mixed, suspended sediment dominated estuaries. The model describes the behaviour of subtidal currents, suspended sediments, nutrients and phytoplankton in a channel geometry. The initial growth of phytoplankton and its spatial distribution is calculated by solving an eigenvalue problem. The growth rates depend on the position in the estuary due to along-estuary variations in nutrient concentration and suspended sediment concentration. The model yields an insight into how the onset of blooms in the model depends on physical and biological processes (turbulent mixing, fresh water discharge, light attenuation, imposed nutrient concentrations at the river and sea side). In particular, the model demonstrates that the joint action of spatial variations in turbidity and in nutrients causes the maximum phytoplankton concentrations to occur seaward of the estuarine turbidity maximum.

Keywords: Estuarine dynamics; Phytoplankton; Turbidity; Stability analysis

1. Introduction

In many estuaries characteristic (spatial and temporal) patterns of phytoplankton (or chlorophyll) concentrations are observed. Field data collected over two decades in San Fransisco Bay (Cloern, 1991) revealed that during each spring phytoplankton blooms occur and that the bloom is more intense during neap tide than during spring tide. Observations of algae in the York river (Sin et al., 1999), a tributary to the Chesapeake Bay (VA), show that during the winter–spring a strong algal bloom is often present in the mid-reach of the mesohaline zone. During the summer a smaller bloom often occurs in the transition zone from fresh water to mesohaline water.

Concepts to explain the behaviour of phytoplankton all use that phytoplankton growth is limited by light and nutrients and that decay of phytoplankton is due to respiration, zooplankton grazing and benthic grazing. It was argued by Sverdrup (1953) that blooms in the ocean occur in early spring when the surface mixed layer becomes so shallow (due to increasing heat input and reduced wind input) that algae can reach areas where sufficient light is available for them to grow. Also, vertical mixing needs to be sufficiently intense that algae can come close to the bottom where nutrient concentrations are largest.

As shown by Lucas et al. (1998), the concepts of Sverdrup cannot be straightforwardly applied to explain phytoplankton growth in coastal plain estuaries because of the different processes that are at work there. First, density stratification in estuaries is usually caused by differences in salinity, not temperature. Second, tides cause strong stirring of phytoplankton. Third, besides the bottom, the discharging river is a main source of nutrients. Fourth, local changes of nutrients and phytoplankton are also affected by horizontal transport processes (Lucas et al., 1999). Finally, light attenuation will be largely influenced by the concentration of suspended sediments in the water (May et al., 2003). The spatial and temporal distribution of suspended sediments is controlled by external forcing conditions, in particular tides and fresh water discharge

*Corresponding author. Tel.: +31 30 2533275; fax: +31 30 2543163.
E-mail address: h.e.deswart@phys.uu.nl (H.E. de Swart).
[1]Present address: Department of Civil and Environmental Engineering, University of Washington, 201 More Hall, Box 352700, Seattle, WA 98195-2700, USA.

0278-4343/$ - see front matter © 2007 Elsevier Ltd. All rights reserved.
doi:10.1016/j.csr.2007.09.006

(Burchard and Baumert, 1998) and by sediment properties (Winterwerp, 2002).

The concepts mentioned above have been incorporated into numerical models with an increasing degree of complexity (see e.g., May et al., 2003). These models have contributed considerable insight into the role of different physical and biological processes on the occurrence of phytoplankton blooms. In particular, the role of time-varying vertical mixing on the tidal and spring–neap time scale has been intensively explored.

For gaining further fundamental understanding of the results of numerical models, it is often helpful to develop and analyse idealised, semi-analytical models. Although the latter often make severe assumptions on the parameterization of processes that are accounted for, they are fast and their results can be analysed and interpreted in relatively straightforward manners. In this paper such a simple model is considered for a well-mixed, suspended sediment dominated estuary. It uses concepts that are similar to those discussed in May et al. (2003), but the focus here is on variations in currents, suspended matter and phytoplankton concentrations in a longitudinal section (from sea to river) rather than in a lateral cross-section. The model is introduced in Section 2 and it is analysed in Section 3. Results are presented and discussed in Sections 4 and 5, respectively, and finally the conclusions are given.

2. Model formulation

2.1. Domain, water motion and SSC distribution

The geometry that will be considered is that of an idealised estuary with a constant width b and constant depth h. A Cartesian coordinate system is chosen, where x, y, z are longitudinal (increasing from sea to river), lateral and vertical coordinates, respectively. Here, $z=0$ is the undisturbed water level.

The equations describing the subtidal currents and suspended sediment concentration (SSC) are equivalent to those used in an accompanying paper (Talke et al., 2007). The flow is described by the steady, linear width-averaged shallow water equations and it is forced by an imposed fresh water discharge at the river mouth and by a horizontal density gradient due to a given salinity distribution in the channel. At the surface the stress vanishes (no wind), whilst at the bottom a no-slip condition is imposed. Salinity is assumed to be well mixed in the vertical. Using results of the above-cited study the along-channel distribution of salinity is modelled as

$$s(x)=\frac{1}{2}s_*\left[1-\tanh\left(\frac{x-x_c}{L}\right)\right]. \tag{1}$$

Here, s_* is the salinity at sea, x_c the position at which the salinity is 50% of its value at sea and x_c+L is a measure of the salt intrusion length (at $x=x_c+L$ the salinity is $0.12s_*$). The density of water, ρ, is calculated from

$$\rho(x)=\rho_0+\beta s, \tag{2}$$

where $\rho_0(\sim 1020\,\mathrm{kgm^{-3}})$ is a constant reference density and $\beta(\sim 0.83\,\mathrm{kgm^{-3}\,psu^{-1}})$ is a coefficient. Turbidity currents induced by gradients in concentration of suspended sediments are neglected in the present model. The Boussinesq approximation is applied, i.e., variations in density are small compared to the reference density. Finally, the rigid lid assumption is made, i.e., elevations of the free surface are ignored, except in maintaining a barotropic pressure gradient.

The longitudinal velocity component $u(x,z)$ that obeys the equations of motion and boundary conditions reads (Officer, 1976)

$$u(x,z)=\frac{gh^3\beta}{48\rho_0 A_v}\frac{\mathrm{d}s}{\mathrm{d}x}\left(1-9\left(\frac{z}{h}\right)^2-8\left(\frac{z}{h}\right)^3\right)+\frac{3Q}{2bh}\left(1-\left(\frac{z}{h}\right)^2\right), \tag{3}$$

where g is the acceleration due to gravity, $A_v(\sim 10^{-3}\,\mathrm{m^2\,s^{-1}})$ is a constant vertical eddy viscosity coefficient and $|Q|(\sim 10^2\,\mathrm{m^3\,s^{-1}})$ is the fresh water discharge. In this model Q has negative values, because the x-axis points to the upstream direction. The terms on the right-hand side describe the currents driven by the horizontal salinity gradient and by fresh water discharge, respectively. The vertical velocity component $w(x,z)$ follows from solving the continuity equation and the result is

$$w(x,z)=-\int_0^z\frac{\partial u}{\partial x}\mathrm{d}z'. \tag{4}$$

Together, u, w describe the classical gravitational (or estuarine) circulation (Hansen and Rattray, 1965).

Mass conservation also implies that the net volume of water transported through any cross-section is constant, i.e.,

$$\int_{-h}^0 u(x,z')\,\mathrm{d}z'=q,\quad q=\frac{Q}{b}. \tag{5}$$

The distribution of suspended sediments is computed from the tidally averaged concentration equation. The particles are assumed to be noncohesive and have a constant settling velocity w_s $(\sim 10^{-3}\,\mathrm{ms^{-1}})$. The horizontal and vertical eddy diffusion coefficients K_h and K_v are assumed to be constant. Typical values are $K_h\sim 10^2\,\mathrm{m^2\,s^{-1}}$ and $K_v\sim 10^{-3}\,\mathrm{m^2\,s^{-1}}$. As shown in Talke et al. (2007) horizontal transport processes play an important role in maintaining an equilibrium distribution of sediment. The solution for the concentration $c(x,z)$ reads

$$c(x,z)=c_b(x)f_c(z),\quad f_c(z)=\exp(-w_s(z+h)/K_v) \tag{6}$$

and the near-bed concentration c_b follows from imposing the morphodynamic equilibrium condition (no net longitudinal transport of sediment), which was first used by Friedrichs et al. (1998). Applying this condition yields the

differential equation

$$J_3\frac{dc_b}{dx}+J_1c_b=0, \tag{7}$$

with

$$J_1(x)=\int_{-h}^{0}u(x,z)f_c(z)\,dz,\quad J_3=-K_h\int_{-h}^{0}f_c(z)\,dz. \tag{8}$$

Note that the two terms that appear in Eq. (7) represent longitudinal transport of sediment due to horizontal diffusion and advective transport, respectively. Since the current and the vertical structure of the sediment concentration are known, the function $J_1(x)$ and coefficient J_3 can be explicitly evaluated. The solution for c_b reads

$$c_b(x)=c_{b,\max}\exp\left[-\int_{x_e}^{x}\frac{J_1(x')}{J_3}dx'\right], \tag{9}$$

where the constant $c_{b,\max}$ is the maximum bottom concentration. This maximum is attained at position $x=x_e$, where $J_1(x_e)=0$.

2.2. Biological module

Let P denote the phytoplankton population density and N the nutrient concentration. To model their dynamics, the following equations are used (see May et al., 2003; Huisman et al., 2006, and references therein for an extensive discussion of the model equations):

$$\frac{\partial P}{\partial t}+\frac{\partial(uP)}{\partial x}+\frac{\partial(wP)}{\partial z}=\mu P-mP+v\frac{\partial P}{\partial z}+K_h\frac{\partial^2P}{\partial x^2}+K_v\frac{\partial^2P}{\partial z^2}, \tag{10a}$$

$$\frac{\partial N}{\partial t}+\frac{\partial(uN)}{\partial x}+\frac{\partial(wN)}{\partial z}=-\alpha\mu P+\delta\alpha mP+K_h\frac{\partial^2N}{\partial x^2}+K_v\frac{\partial^2N}{\partial z^2}. \tag{10b}$$

Here, $\mu=\mu(N,I)$ is the specific growth factor of the phytoplankton as a function of nutrient availability N and light intensity I, m the specific loss rate of the phytoplankton, v the phytoplankton sinking velocity, K_v the vertical turbulent diffusivity, α the nutrient content of the phytoplankton and δ the proportion of nutrient in dead phytoplankton that is recycled. Typical values of the parameters will be discussed later on.

The specific growth factor $\mu(N,I)$ is modelled as

$$\mu(N,I)=\mu_{\max}\left(\frac{N}{H_N+N}\right)\left(\frac{I}{H_I+I}\right), \tag{11}$$

where $\mu_{\max}$ is the maximum specific growth factor and H_N and H_I are the half-saturation constants for nutrient-limited and light-limited growth, respectively. The light intensity I decreases exponentially with depth according to Lambert–Beer's law:

$$I=I_0\exp\left(k_{\rm bg}z-k_c\int_z^0c(x,z')\,dz'-k_{\rm phyto}\int_z^0P(t,z')\,dz'\right). \tag{12}$$

In this expression I_0 is the incident light intensity and $k_{\rm bg}$, k_c and $k_{\rm phyto}$ are the specific light absorption coefficient due to the presence of background turbidity, suspended sediment and phytoplankton in the water, respectively. Note that z-values are negative (between $-h$ and 0).

Boundary conditions are that $N(x=0)=N_0$ and $N(x\to\infty)=N_\infty$, i.e., nutrient concentrations are prescribed at the seaside and riverine side, respectively. Furthermore, a no-flux condition for nutrients through the bottom and free surface is used. For the phytoplankton, we assume zero-flux boundary conditions at the bottom and free surface and vanishing concentration gradients on both the seaward and riverine boundary.

In order to simulate phytoplankton blooms we allow both nutrients and phytoplankton to be functions of time. Because the equations are averaged over a tidal period N and P vary on the subtidal time scale.

3. Analysis of the biological equations: initial behaviour of blooms

Eqs. (10a)–(10b) are two coupled nonlinear differential equations and obtaining general solutions requires the use of numerical methods. Zagaris et al. (2007) recently pointed out that the conditions under which phytoplankton blooms occur can be systematically explored by considering only the stability properties of a state without phytoplankton with respect to small perturbations in N and P. This allows for a linearisation of the equations and solutions can be found by analytical methods. Zagaris et al. (2007) showed that their model reproduces the stability bounds of the model of Huisman et al. (2006), which describes the nonlinear behaviour of nutrients and phytoplankton in a single water column in the deep sea. Here, we employ their idea to the estuarine model that has been discussed in the previous section.

First, scaling of Eqs. (10a)–(10b) shows that nonlinear advection terms and horizontal diffusion terms are an order of magnitude smaller than terms related to vertical diffusion and local growth and decay processes. Ignoring these small contributions it appears that the system allows for a *steady* basic state $P=\bar{P}=0$, $N=\bar{N}(x)$, which is characterised by the absence of phytoplankton and by nutrients which are well mixed over the vertical. The longitudinal structure of $\bar{N}(x)$ is obtained by integrating the full Eq. (10b) over the vertical and applying the boundary conditions at the bottom and free surface, as well as constraint (5) on the current. The

result is

$$\frac{\mathrm{d}}{\mathrm{d}x}\left(q\bar{N} - K_h h\frac{\mathrm{d}\bar{N}}{\mathrm{d}x}\right) = 0. \tag{13}$$

The solution of this equation that obeys the boundary conditions (see Section 2.2) reads

$$\bar{N}(x) = N_\infty + (N_0 - N_\infty)\exp\left(\frac{qx}{K_h h}\right). \tag{14}$$

Note that in this expression q has a negative value. The light intensity in the basic state is given by

$$\bar{I}(x,z) = I_0 \exp\left[-k_{\mathrm{bg}}z - k_c\int_0^z c(x,z')\,\mathrm{d}z'\right], \tag{15}$$

with $c(x,z')$ the known SSC.

Next, the dynamics of perturbations evolving on this basic state are considered. Thus, solutions of the form

$$P = P', \quad N = \bar{N}(x) + N'$$

are substituted in Eqs. (10a)–(10b). These perturbations are assumed to be small, meaning that contributions which are nonlinear in P', N' can be ignored. This method is known as a *linear stability analysis*. If only the dominant terms in these equations are maintained the resulting equations are

$$\frac{\partial P'}{\partial t} = \mu(\bar{N},\bar{I})P' - mP' + v\frac{\partial P'}{\partial z} + K_v\frac{\partial^2 P'}{\partial z^2}, \tag{16a}$$

$$\frac{\partial N'}{\partial t} = -\alpha\mu(\bar{N},\bar{I})P' + \delta\alpha m P' + K_v\frac{\partial^2 N'}{\partial z^2}. \tag{16b}$$

Note that the equation for P' is decoupled from that of N', so the equations can be separately solved.

Both equations allow for solutions that vary exponentially in time, with an as yet unspecified initial growth rate λ:

$$(N', P') = \Re\{(\hat{N},\hat{P})\mathrm{e}^{\lambda t}\}.$$

Here $\Re$ denotes the real part of the solution and $\hat{N},\hat{P}$ govern the spatial structure of the solutions. Substituting these solutions in the equations for N', P' yields

$$K_v\frac{\partial^2\hat{P}}{\partial z^2} + v\frac{\partial\hat{P}}{\partial z} = -(\mu - m - \lambda)\hat{P}, \tag{17a}$$

$$K_v\frac{\partial^2\hat{N}}{\partial z^2} - \lambda\hat{N} = \alpha(\mu - \delta m)\hat{P}. \tag{17b}$$

The equation for $\hat{P}$, together with its boundary conditions, defines for each longitudinal position x an *eigenvalue problem*. Thus, λ are the eigenvalues and $\hat{P}$ are the corresponding eigenfunctions. A solution for a specific λ and corresponding eigenfunction is called a mode. Apparently, x enters the equation only as a parameter, so the initial growth rate λ depends parametrically on x. This eigenvalue problem can be straightforwardly cast as a Sturm-Liouville problem, which implies that the eigenvalues and eigenfunctions are real.

Once the solutions for $\hat{P}$ are known, the solutions for the nutrient perturbations can also be calculated. However, because N' represents only a small correction to the nutrient concentration $\bar{N}(x)$ of the basic state, these perturbations will not be considered.

In the experiments discussed hereafter solutions for $\lambda(x)$ and the corresponding eigenfunctions were obtained by discretizing equation (17a) on a regular grid. The resulting matrix eigenvalue problem was solved numerically with a standard LAPACK routine.

4. Results

In order to gain systematic understanding of the behaviour of the model several experiments were designed such that they describe situations with an increasing degree of complexity. Two main cases will be distinguished, which correspond to biological conditions that are horizontally uniform and nonuniform, respectively.

4.1. Horizontally uniform conditions

The first case is obtained when $c_{b,\max} = 0$ (no suspended matter available) and the nutrient concentration is constant, $N = N_*$. The latter situation implies that $N_0 = N_\infty = N_*$. In this situation the phytoplankton dynamics are not affected by currents and SSC.

Values for the input parameters, which are representative for a typical well-mixed suspended sediment dominated estuary at midlatitudes, are given in Table 1. Setting these parameter values defines the default case. Although the parameters α, δ and k_{phyto} occur in the basic model, solutions of the eigenvalue problem (17a), which describes

Table 1
Biological quantities and parameter values for a typical estuary

Dimensional model

Quantity	Symbol	Value
Water depth	h	7 m
Vertical eddy diffusion coefficient	K_v	$1\times10^{-3}\,\mathrm{m^2\,s^{-1}}$
Surface light intensity	I_0	$400\,\mu\mathrm{mol\,photons\,m^{-2}\,s^{-1}}$
Nutrient concentration far upstream	N_∞	$10\,\mathrm{mmol\,m^{-3}}$
Nutrient content of phytoplankton	α	$1\times10^{-6}\,\mu\mathrm{mol\,N\,cell^{-1}}$ (a)
N recycling coefficient	δ	0.5 (a)
Specific loss rate	m	$2.8\times10^{-6}\,\mathrm{s^{-1}}$ (a)
Maximum specific growth factor	$\mu_{\max}$	$1.1\times10^{-5}\,\mathrm{s^{-1}}$ (a)
Sinking velocity phytoplankton	v	$1.16\times10^{-5}\,\mathrm{m\,s^{-1}}$ (a)
Half-saturation constant of N-limited growth	H_N	$0.025\,\mathrm{mmol\,m^{-3}}$ (a)
Half-saturation constant of I-limited growth	H_I	$20\,\mu\mathrm{mol\,photons\,m^{-2}\,s^{-1}}$ (a)
Light absorption due to background turbidity	k_{bg}	$1.0\,\mathrm{m^{-1}}$ (b)
Light absorption due to SSC	k_c	$50.0\,\mathrm{m^{-1}\,kg^{-1}\,m^3}$ (b)
Light absorption coefficient of phytoplankton	k_{phyto}	$6\times10^{-10}\,\mathrm{m^2\,cell^{-1}}$ (a)

Sources are (a) Huisman et al. (2006), (b) May et al. (2003).

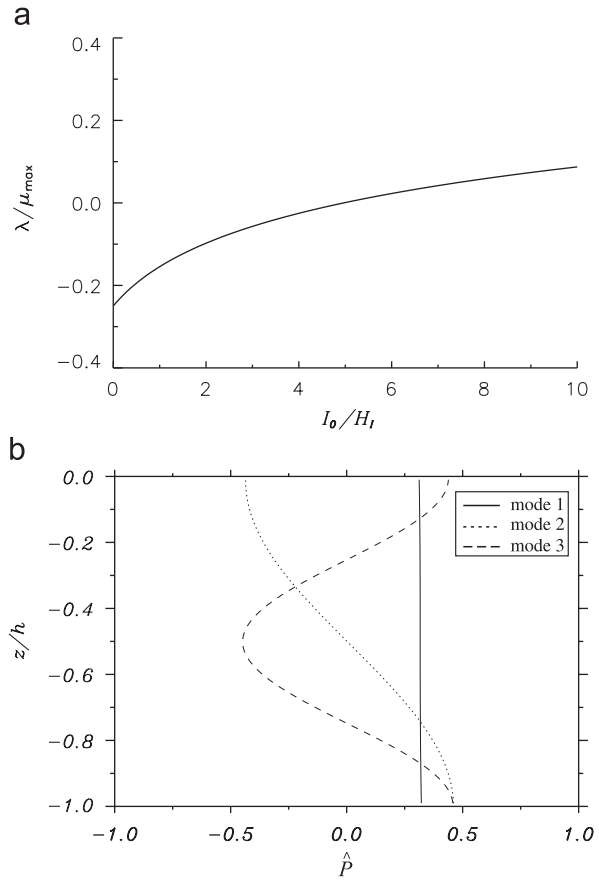

Fig. 1. (a) First eigenvalue λ_1 (scaled by maximum specific growth factor μ_{max}) versus surface light intensity I_0 (scaled by the half saturation parameter H_I). (b) Vertical structure of the eigenfunctions that correspond to eigenvalues λ_1 (solid curve), λ_2 (dotted curve) and λ_3 (dashed curve).

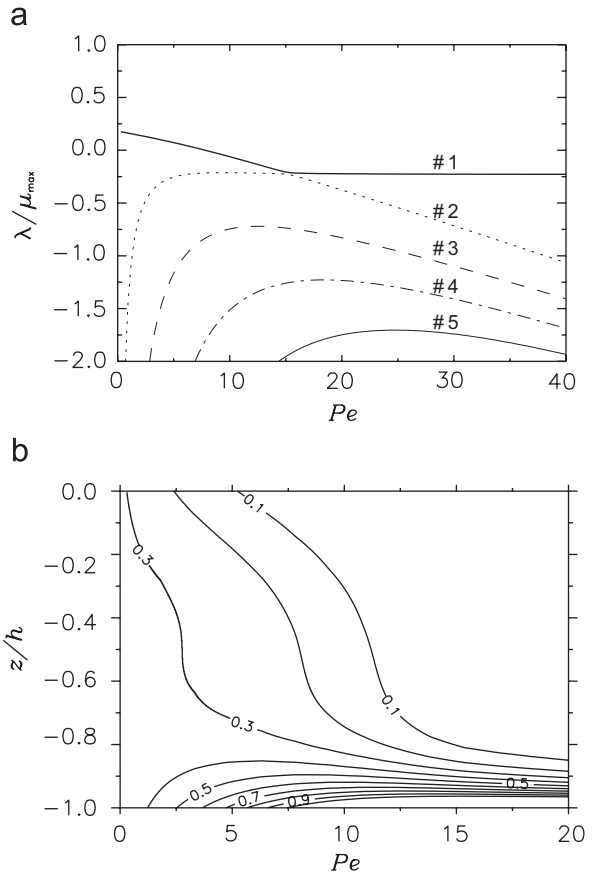

Fig. 2. (a) Eigenvalues $\lambda_1-\lambda_5$ (scaled by maximum phytoplankton growth factor μ_{max} and ordered according to their values) versus phytoplankton vertical Péclet number $Pe = vh/K_v$ (parameter K_v is varied here). (b) Contour plot of eigenfunction that corresponds to largest eigenvalue λ_1 in the $Pe-(z/h)$ plane.

the initial growth of phytoplankton, do not depend on these parameters.

First, we investigate the dependence of phytoplankton growth on the surface light intensity I_0. In Fig. 1a the largest eigenvalue λ_1 is shown as a function of I_0. This subfigure shows that phytoplankton will grow if $(I_0/H_I) > 4.97$, hence if the surface light intensity exceeds 99.4 μmol photons $m^{-2}\,s^{-1}$. As is to be expected, the growth rate monotonically increases with increasing light intensity. For all values of I_0 shown here λ_1 is the only positive eigenvalue, which implies that there is only one initially growing mode. In case that the surface irradiance has the default value $I_0 = 400\,\mu$mol photons $m^{-2}\,s^{-1}$ the e-folding time scale $T_{pref} = \lambda_1^{-1}$ of the growing mode is ~5 days.

Fig. 1b shows the vertical structure of the first three eigenfunctions for the default case. Note that the growing phytoplankton mode, represented by the solid line, is almost uniform over the water column. Another interesting observation is that the second and third eigenfunctions change sign over the vertical. Mathematically, this is to be expected: the number of zero-crossings will increase with increasing mode number. Physically, this result means that phytoplankton concentrations (which must be positive) can not be described by eigenmodes 2 and 3 themselves. However, a linear combination of modes, such that concentration remains positive, may allow for growth to occur.

Another important parameter that affects the phytoplankton growth is

$$Pe = \frac{vh}{K_v}, \tag{18}$$

which is the phytoplankton vertical Péclet number. It determines the ratio between the time scales related to turbulent diffusion and settling, respectively. Fig. 2a displays the dependence of the eigenvalues on Pe in this model. The largest eigenvalue decreases monotonically with increasing Pe and approaches a limiting value (which is negative in this case) for large Pe. So, one so-called bifurcation point is found, at which the stability of the basic state changes from unstable to stable. The other eigenvalues show a different dependence on Pe. For small Pe they are strongly negative and they increase with increasing Pe. After attaining a maximum they subsequently decrease with Pe and the difference between successive eigenvalues becomes small. Interestingly, the

maximum of λ_2 coincides with the minimum of λ_1, so two modes exchange preference at this point. The reason why eigenvalue λ_1 behaves so differently from the other eigenvalues will be presented in the next section.

The corresponding phytoplankton distribution (Fig. 2b) shows that with increasing values of Pe the phytoplankton becomes more and more trapped near the bottom. This tendency is understandable because increasing Pe means that downward settling of phytoplankton becomes larger with respect to upward vertical mixing of phytoplankton. For $2<Pe<8$ the phytoplankton concentration of the first, dominant mode has a remarkable vertical structure. Starting from a high value at the bottom it first rapidly decreases, then it becomes almost constant and towards the surface it decreases more rapidly again. This property of the eigenfunction will be explained later on.

4.2. Nonuniform conditions: role of currents and SSC

We now systematically investigate the dependence of phytoplankton growth on hydrodynamic forcing conditions, sediment properties and on spatial variations in the nutrient concentration.

The default values of the water depth and the biological parameters are given in Table 1. However, the light attenuation coefficient due to background turbidity in the water is set to $k_{bg} = 0.045\,\mathrm{m}^{-1}$, following Huisman et al. (2006), such that the light attenuation will be mainly due to SSC. The physical parameters are $s_* = 30$ psu, $x_c = 25$ km, $L = 50$ km, $A_v = 1\times10^{-3}\,\mathrm{m^2\,s^{-1}}$ and $q = -0.03\,\mathrm{m^2\,s^{-1}}$. The settling velocity of the sediment particles is $w_s = 1\times10^{-3}\,\mathrm{m\,s^{-1}}$. This implies that the e-folding depth scale of SSC is $\delta_* = (A_v/w_s) = 1$ m. For the present depth of 7 m values of surface SSC are a factor $e^{-7} \simeq 0.91\times10^{-3}$ smaller than bottom SSC. The default value for the maximum SSC at the bottom, $c_{b,\max}$ is chosen as $c_{b,\max} = 5\,\mathrm{kgm^{-3}}$.

Fig. 3a displays a contour plot of the specific growth factor μ of phytoplankton for the default parameter setting. It shows that the strongest decay of this growth factor with depth occurs at location $x/L \simeq 1.6$, i.e., at about 80 km from the seaward boundary. This is because here the SSCs attain their largest values, thereby causing the strongest attenuation of light with increasing depth.

In Fig. 3b the spatial variation of the first eigenvalue λ_1, which represents the largest initial growth rate of phytoplankton concentration in the channel, is plotted for different values of the maximum SSC bottom concentration $c_{b,\max}$. The other eigenvalues have negative values. By moving from sea to river, the initial growth rate decreases due to increasing SSC, reaches a minimum at the location of the estuarine turbidity maximum (ETM) and then increases again due to decreasing SSC. Once $c_{b,\max}$ exceeds a critical value (in this case a value of $\simeq 7\,\mathrm{kgm^{-3}}$) there is a region around the ETM where phytoplankton will not grow.

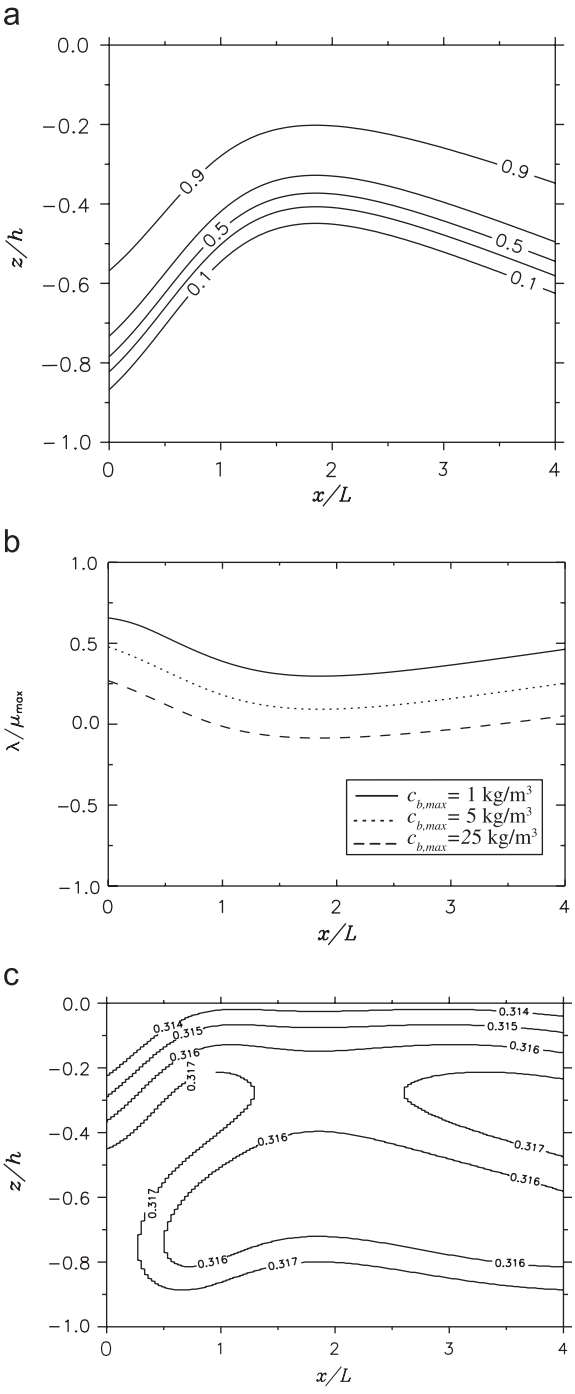

Fig. 3. (a) Contour plot of specific growth factor of phytoplankton in the channel. Here, x is the vertical coordinate (scaled by length L) and z the vertical coordinate (scaled by depth h). (b) Initial growth rate of phytoplankton (scaled by maximum specific growth factor $\mu_{\max}$) versus the distance to the seaward boundary (scaled by length L) for $c_{b,\max} = 1\,\mathrm{kgm^{-3}}$ (solid curve), $c_{b,\max} = 5\,\mathrm{kgm^{-3}}$ (dotted curve) and $c_{b,\max} = 25\,\mathrm{kgm^{-3}}$ (dashed curve). (c) Contour plot of the spatial distribution of the fastest growing phytoplankton mode ($c_{b,\max} = 5\,\mathrm{kgm^{-3}}$).

The spatial structure of the corresponding eigenfunction is shown in Fig. 3c. It reveals that, while moving from sea to river, the vertical level at which the maximum phytoplankton concentration occurs shifts from the bottom to higher levels. An explanation for this phenomenon will be

given in the next section. Note that vertical variations in the eigenfunction are weak for the presently chosen values of the parameters.

The longitudinal distribution of the initial growth rate also depends on parameters q, x_c and L, which determine the spatial structure of SSC. In Fig. 4a curves of $\lambda(x)$ are shown for different values of the fresh water discharge per unit width, $|q|$ and a fixed value $c_{b,\max} = 5\,\mathrm{kgm}^{-3}$ for the maximum bottom concentration. With increasing (decreasing) $|q|$, the location of the ETM shifts downstream (upstream), which causes the preferred region of phytoplankton growth to shift upstream (downstream). In Fig. 4b and Fig. 4c curves are shown of $\lambda(x)$ for different values of parameters x_c and L, respectively. As discussed in Section 2 they determine the locations at which the salinity is 50% and 12% of its value at sea. For larger x_c and/or L salinity gradients become weaker in the downstream region of the estuary, thereby causing the ETM to shift seaward. Consequently, the growth of phytoplankton becomes smaller (larger) in the downstream (upstream) region. The opposite trends are found if smaller values of x_c and/or L are considered.

Fig. 5a shows the longitudinal variation of the growth rate of phytoplankton for different values of the settling velocity w_s. In Fig. 5b similar curves are shown, but for different values of the turbulent eddy viscosity coefficient A_z and eddy diffusion coefficient K_v. Varying the settling velocity implies that the sediment Péclet number changes, but the Péclet number of the phytoplankton remains unchanged. When the turbulent eddy diffusion coefficient K_z is varied both Péclet numbers change. Moreover, because it is assumed here that $K_v = A_v$, the spatial pattern of the estuarine circulation changes, which affects the SSC distribution.

In the case that w_s is increased (decreased), i.e., coarser (finer) grains, the sediment gets more (less) trapped to the bottom and, thus, light will penetrate more (less) deep in the water. This results in an enhanced (reduced) phytoplankton growth. The dependence on eddy viscosity and eddy diffusion is more subtle. When turbulent mixing and diffusion are enhanced three important changes occur. First, the density-driven flow weakens, as can be seen from the first term on the right-hand side of Eq. (3). This causes the ETM to shift seaward. Second, the sediments in suspension extend over a larger part of the water column, thereby causing stronger light attenuation. Third, the vertical phytoplankton Péclet number will become smaller and phytoplankton will be more uniformly distributed over depth. The final result is that phytoplankton growth becomes smaller, in particular in the seaward part of the domain. The opposite occurs in case turbulent mixing and diffusion are reduced.

Fig. 6a shows the longitudinal variation of the growth rate of phytoplankton for different values of the nutrient concentrations N_0 (at sea) and N_∞ (at the river). It reveals that, while moving downstream, decreasing nutrient concentrations can cause phytoplankton growth to become

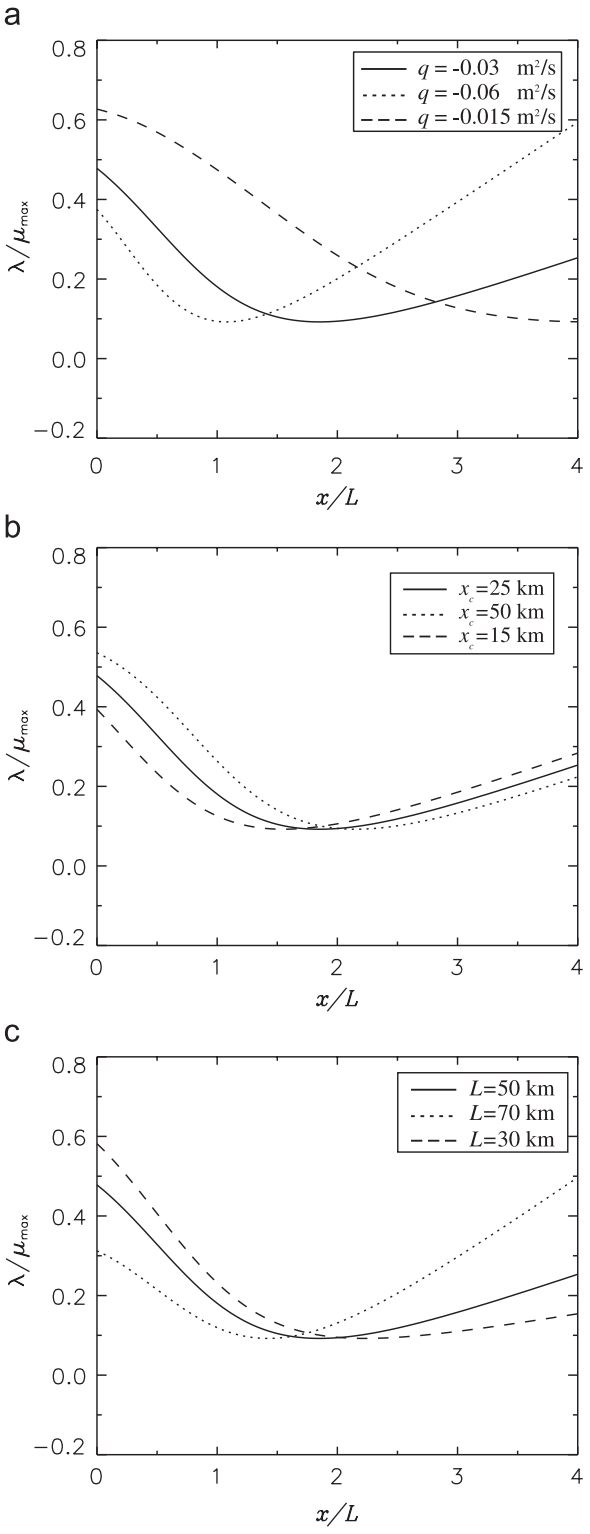

Fig. 4. (a) As Fig. 3a, but for $c_{b,\max} = 5\,\mathrm{kgm}^{-3}$ and $q = -0.03\,\mathrm{m}^2\,\mathrm{s}^{-1}$ (solid curve), $q = -0.06\,\mathrm{m}^2\,\mathrm{s}^{-1}$ (dotted curve) and $q = -0.015\,\mathrm{m}^2\,\mathrm{s}^{-1}$ (dashed curve). (b) As above, but for $x_c = 25$ km (solid curve), $x_c = 40$ km (dotted curve) and $x_c = 15$ km (dashed curve). (c) As above, but for $L = 50$ km (solid curve), $L = 70$ km (dotted curve) and $L = 30$ km (dashed curve).

nutrient limited. Consequently, the maximum phytoplankton concentrations will occur at a location between the seaward boundary and the location of the ETM. Finally,

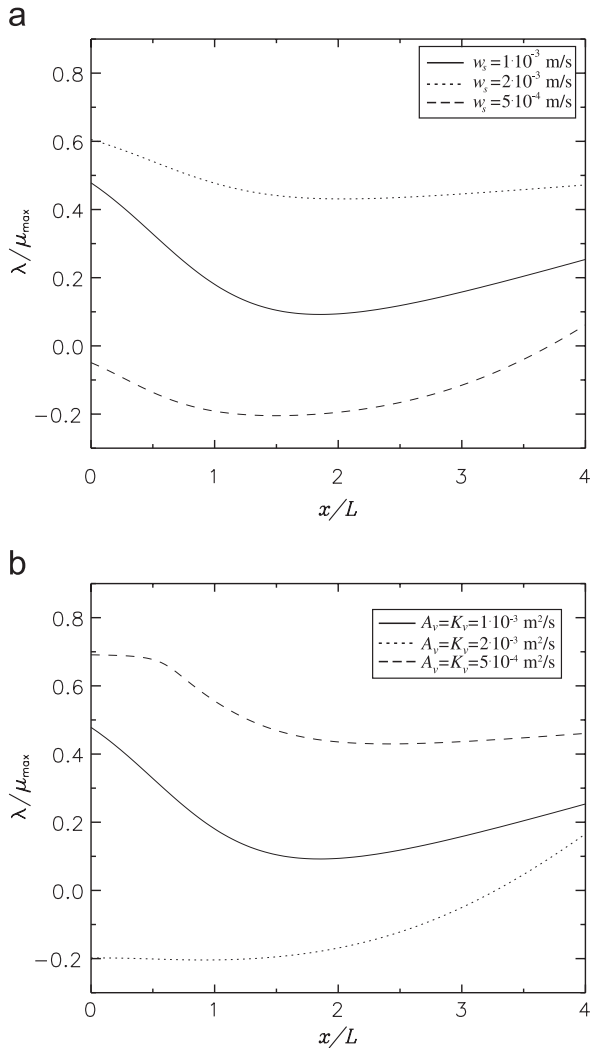

Fig. 5. (a) As Fig. 3a, but for $w_s = 1 \times 10^{-3}\,\mathrm{ms}^{-1}$ (solid curve), $w_s = 2 \times 10^{-3}\,\mathrm{ms}^{-1}$ (dotted curve) and $w_s = 5 \times 10^{-4}\,\mathrm{ms}^{-2}$ (dashed curve). (b) As above, but for $A_v = K_v = 1 \times 10^{-3}\,\mathrm{m}^2\,\mathrm{s}^{-1}$ (solid curve), $A_v = K_v = 2 \times 10^{-3}\,\mathrm{m}^2\,\mathrm{s}^{-1}$ (dotted curve) and $A_v = K_v = 5 \times 10^{-4}\,\mathrm{m}^2\,\mathrm{s}^{-1}$ (dashed curve).

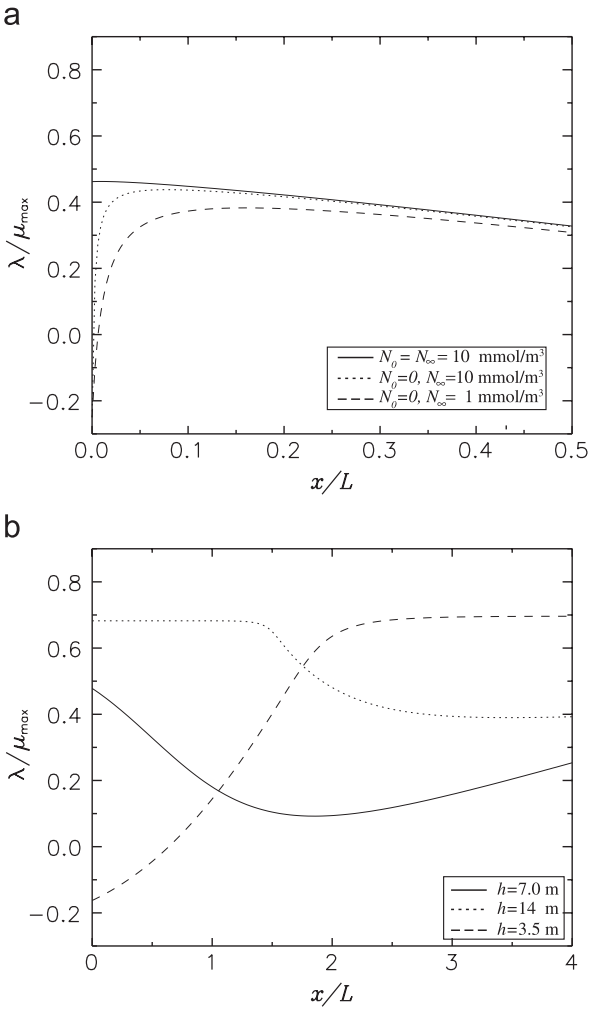

Fig. 6. (a) As Fig. 3a, but for $N_0 = N_\infty = 10\,\mathrm{mmol\,m}^{-3}$ (solid curve), $N_0 = 0, N_\infty = 10\,\mathrm{mmol\,m}^{-3}$ (dotted curve) and $N_0 = 0, N_\infty = 1\,\mathrm{mmol\,m}^{-3}$ (dashed curve). (b) As above, but for depth $h = 7\,\mathrm{m}$ (solid curve), $h = 14\,\mathrm{m}$ (dotted curve) and $h = 3.5\,\mathrm{m}$ (dashed curve).

Fig. 6b shows the along-estuary variation of initial phytoplankton growth rates for different depths h. If a larger depth is considered, the density-driven flow becomes stronger and the ETM shifts landward. Furthermore, the thickness of the suspended sediment layer remains unchanged, such that at a fixed location in the water column the light intensity will be larger. Thus, phytoplankton grows more rapidly, in particular in the seaward part of the domain.

5. Discussion

5.1. Interpretation of results

Below, we discuss and explain some of the results of the previous section. All arguments are based on Eq. (16a) that governs the initial growth of phytoplankton. It shows that the local mass of phytoplankton per volume changes due to local mass gain and loss (first two terms on the right-hand side) and due to the vertical gradient of the phytoplankton flux component

$$F = -\left(vP' + K_v \frac{\partial P'}{\partial z}\right) \tag{19}$$

(last two terms on the right-hand side of Eq. (16a)). Note that F consists of two components, the settling flux (directed downward) and the vertical diffusive flux. The boundary conditions are that this flux vanishes at both the sea surface and at the bottom. Since there is no flux of phytoplankton entering or leaving the water column the amount of phytoplankton mass stored in a water column with unit surface area is only affected by the integrated gain and loss terms. This can also be seen by integrating Eq. (16a) over the depth and using the boundary conditions, yielding

$$\frac{\partial}{\partial t}\int_{-h}^{0} P'\,\mathrm{d}z = \int_{-h}^{0} [\mu(z) - m]P'\,\mathrm{d}z. \tag{20}$$

From Eq. (20) several conclusions can be drawn. First, it shows that a necessary and sufficient condition for growth of phytoplankton is that the depth-averaged specific growth factor, $\bar{\mu}$, exceeds the specific loss rate m. In Section 3 it was shown that in this model the specific growth factor μ at a fixed location x is determined only by the light intensity, which decreases towards the bottom. Nutrients do not affect the vertical structure of μ because they are uniformly distributed in the water column. Consequently, the value of $\bar{\mu}$ depends on the water depth, the light absorption coefficient due to background turbidity, k_{bg} and on the amount of light that is attenuated due to the presence of suspended sediments in the water. In the case that no SSC is considered (Section 4.1), it appears that $\bar{\mu}$ is a monotonically decreasing function of depth h. Thus, if the depth exceeds a critical value no initial growth of phytoplankton will occur.

In the case that light is also attenuated by SSC (Section 4.2) the dependence of $\bar{\mu}$ on depth h is more complicated. This is because attenuation of light due to SSC in the upper part of the water column will reduce with increasing depth, because the sediment becomes more trapped near the bottom (the Péclet number is larger). This favours increase of $\bar{\mu}$ with depth. As long as depths are smaller than k_{bg}^{-1} (in this case $\sim$25 m) this effect exceeds the decrease of $\bar{\mu}$ that is due to light absorption by background turbidity. This is why the phytoplankton growth rates shown in Fig. 5b are larger for larger depth. Only for depths of order k_{bg}^{-1} and larger, the growth rates will decline with depth, until again a critical depth is reached beyond which no growth of phytoplankton occurs.

As shown in Fig. 2 the largest eigenvalue monotonically decreases with increasing values of the Péclet number Pe. To understand this behaviour consider first the case of a small Péclet number. According to definition (18) this means that the time scale of vertical diffusion is much smaller than the time scale of settling. As a consequence the phytoplankton will be distributed almost uniformly over the water column and Eq. (20) reduces to

$$\frac{\partial P'}{\partial t}h = \left[\int_{-h}^{0} \mu(z)\,\mathrm{d}z - mh\right]P'. \tag{21}$$

Since $P' \sim \exp(\lambda_1 t)$, it follows that $\lambda_1 \sim (\bar{\mu} - m)$ for small Péclet numbers.

In case of large Pe the phytoplankton is trapped in a thin boundary layer (thickness of order h/Pe) and, hence, the gain and loss of mass will take place only in that layer. Thus, Eq. (20) can be approximated by

$$\frac{\partial}{\partial t}\int_{-h}^{0} P' dz = (\hat{\mu} - m)\int_{-h}^{0} P'\,\mathrm{d}z, \tag{22}$$

where $\hat{\mu} = \mu(z = -h)$ is the specific growth factor at the bottom. Again, substitution of a solution $P' \sim \exp(\lambda_1 t)$ yields $\lambda_1 \sim (\hat{\mu} - m)$ for large Péclet numbers. Obviously, for intermediate values of Pe the largest eigenvalue will be between these extreme values.

Another remarkable aspect of Fig. 2a is that the largest eigenvalue has quite a different dependence on the Péclet number than all other eigenvalues. To explain this it is useful to analyse the eigenvalue problem (17a) for a constant specific growth factor $\mu = \bar{\mu}$. Physically this means that we analyse the local mass balance of phytoplankton in a water column in which attenuation of light is negligible. The advantage of this assumption is that the eigenvalue problem allows for analytical solutions. As is shown in Appendix A, two types of eigenmodes are obtained. The first is a mode that has an eigenvalue $\lambda_1 = \langle \mu - m \rangle$, independent of the Péclet number. Its vertical structure is characterised by a vanishing vertical flux F (where F is defined in Eq. (19) above) in the entire water column, which results in an exponential distribution of phytoplankton population density that increases towards the bottom. The other eigenmodes follow from a different root of the eigenvalue problem and they are smaller than that of the first mode. These eigenvalues are characterised by the fact that they become strongly negative for both small and large values of the Péclet number. For intermediate Pe they attain a local maximum. Further, they have a mixed oscillatory-exponential structure in the vertical.

Next, we present arguments for why Figs. 2b and 3c show that the phytoplankton distribution of the first mode over the vertical can have a local extremum at some distance from the bed. This is due to the decreasing specific growth factor μ while moving from sea surface to bottom. As was discussed above, in the case that μ is constant the vertical distribution is characterised by a vanishing flux F in the entire water column, i.e., everywhere local loss of phytoplankton is compensated by local gain. Once μ varies with z this balance is no longer possible. Assume that $\mu = \bar{\mu} + \tilde{\mu}(z)$, where $\tilde{\mu}$ is small compared to the constant $\bar{\mu}$. In that case the local mass balance for the first mode reads

$$\frac{\partial F}{\partial z} = \tilde{\mu} P'. \tag{23}$$

In the upper part of the water column the specific growth factor is larger than its depth-averaged value, hence $\tilde{\mu} > 0$. The mass balance (23) shows that in this area the vertical flux of phytoplankton is divergent. As $F = 0$ at the sea surface this means that the flux is negative in this area; hence, settling prevails over vertical diffusion. Using the definition of F it follows that

$$\frac{-1}{P'}\frac{\partial P'}{\partial z} < 1, \tag{24}$$

so the vertical gradient of P' will be smaller than that obtained for $\tilde{\mu} = 0$.

Likewise, close to the bottom $\tilde{\mu}$ is negative and thus the flux F is convergent. As $F = 0$ at the bottom it follows that F is also negative in this area and again, the vertical gradient of P' is smaller than in the situation that $\tilde{\mu} = 0$. Fig. 3c reveals that this gradient of P' changes sign, so that

in part of the water column P' increases from the bottom towards the surface, such that a local extremum of P' above the bottom occurs.

A final remarkable aspect of this model that deserves some discussion is that it predicts that phytoplankton growth will reduce if turbulent stirring and mixing are enhanced. This seems in contradiction to field observations (Cloern, 1991), which indicate that phytoplankton blooms usually occur around spring tide, when tidal stirring is maximum. The reason for this discrepancy is that our model predicts that, for increasing vertical eddy diffusion, suspended sediments become more uniformly distributed over the water column. However, in the results shown in Fig. 5 the same value of the maximum bottom concentration was kept. This means that, when doubling K_v, the total amount of suspended sediments in the water column is almost doubled as well. If the total amount of sediment that is suspended in the water column would be kept fixed, then phytoplankton growth rates in the upstream part of the domain become larger than those obtained for the default case.

5.2. Model limitations

Several strong assumptions have been made in developing our model. Most of them we mention only briefly, because they are extensively discussed in Talke et al. (2007). First, tides are not explicitly accounted for. Thus, processes like nonlinear advection of momentum and material by tidal currents, depth-dependent friction and net mass transport by tidal currents are ignored and time-varying mixing of momentum and diffusion of material are neglected. Many studies (cf. Postma, 1954; Jay and Musiak, 1994; Li and O'Donnell, 1997; Schuttelaars and De Swart, 2000; May et al., 2003; Lerczak and Geyer, 2004) have shown that these processes affect subtidal flow, SSC distribution and/or the distribution of phytoplankton. Second, sediment particles are assumed to be noncohesive, whereas in many natural estuaries the sediment is cohesive. This implies processes like flocculation which, again, can strongly influence the hydrodynamics (through mixing), as well as SSC (Winterwerp, 2002) and phytoplankton distributions. Also, gradients in SSC are assumed to be sufficiently small such that turbidity currents can be ignored with respect to currents driven by salt gradients and fresh water discharge. This is a noticeable difference with the paper of Talke et al. (2007) which considers subtidal flow and SSC in highly turbid model estuaries. Third, eddy viscosity coefficients and eddy diffusion coefficients are not only assumed to be constant in time, but also in space and the salinity field is considered as given (no feedback from flow to density field). Both field observations (Helder and Ruardij, 1982; Monismith et al., 2002) and theoretical considerations (Zimmerman, 1986, and references herein) indicate that, in particular, horizontal eddy viscosity coefficients show strong along-estuary variations.

The fourth important limitation is that biological variables do not affect the hydrodynamics and the distribution of SSC. In reality, feedbacks from the biology to the sediment dynamics are certainly important (Widdows et al., 2000) and this is currently a topic of intense research (cf. Tolhurst et al., 2006). Finally, our model results only yield information about the initial growth of phytoplankton, which behaves exponentially in time. In this phase the feedback from phytoplankton to light is negligible. However, when phytoplankton concentrations become large they will cause strong attenuation of light, which causes P' to have finite amplitude behaviour over the long term. Finally, we remark that the present model does not yield information about the along-estuary distribution of the eigenmodes. In fact, eigenfunctions can be calculated at any position x in the domain, but the amplitude is only known up to an arbitrary constant $A(x)$. In principle there is a method to solve for this unknown constant, but that is beyond the scope of the present paper.

6. Conclusions

In this paper we presented and analysed an idealised model with the objective to gain more knowledge about spatial variations of phytoplankton growth in well-mixed suspended sediment dominated estuaries. The domain considered is a channel having a constant depth and width and extending from the seaward boundary (salt water) to the upstream boundary (fresh water). The dynamics of phytoplankton are described by a mass balance equation which involves advection, settling, turbulent diffusion and specific growth and decay terms. The specific growth factor of phytoplankton is limited by the availability of nutrients and light. The distribution of nutrients is calculated by solving a mass balance equation that involves similar terms as the phytoplankton equation.

The attenuation of light is modelled as a function of background turbidity, amount of suspended sediments and of phytoplankton concentration in the water column. The suspended sediment concentration (SSC) follows from mass conservation and depends on the hydrodynamic conditions and sediment properties. Here, noncohesive fine sediment is considered and the subtidal flow is governed by fresh water discharge and a prescribed horizontal density gradient. Tides act only to mix momentum, diffuse material and stir sediment from the bottom. Turbulent eddy viscosity and eddy diffusion coefficients are assumed to be constants, both in space and time. Thus, the equations for the current and SSC follow from those used by Festa and Hansen (1978) in the limit of weak advection (with respect to diffusion). In this paper the SSC pattern is calculated by imposing the condition of vanishing net horizontal transport of sediment (morphodynamic equilibrium).

It was demonstrated that the system allows for a basic state which is characterised by the absence of phytoplankton and a vertically homogeneous nutrient concentration, which has a known along-estuary distribution. Upon

introducing small perturbations in phytoplankton and nutrient concentration, equations were derived that govern the initial evolution of these perturbations. The final result was an eigenvalue problem for the phytoplankton concentration P', where the eigenvalues represent the initial growth rate of the free modes whose vertical structure is given by the corresponding eigenfunctions.

Analysis of the eigenvalue problem revealed that phytoplankton will grow, due to an inherent feedback mechanism, if nutrient concentration and light intensity are sufficiently high (the latter occurs if SSC is sufficiently low) and if the ratio of time scales of turbulent mixing to the settling of phytoplankton are sufficiently large. For a range of parameter values that are representative of typical estuaries, the number of growing modes varies between 0 and 2. The eigenvalues vary when moving from the seaward boundary towards the river, because the currents determine the along-estuary variation of the background (basic state) nutrient concentration and of SSC, which in turn affect the local specific growth factor of phytoplankton. A sensitivity study demonstrated that the actual spatial pattern of the largest initial growth rate, apart from depending on biological parameters and depth, strongly depends on the fresh water discharge and salinity distribution, sediment properties and the eddy diffusion coefficients. For realistic values of the parameters the preferred region of phytoplankton growth was found between the seaward boundary and the estuarine turbidity maximum (ETM). This is because near the seaward boundary the phytoplankton growth is nutrient limited, whereas near the ETM the growth is light limited. As the SSC distribution is asymmetric with respect to the location of the ETM (values of SSC are larger on the landside than on the seaside) the phytoplankton prefers the region seaward of the ETM.

The model predicts that the growth of phytoplankton increases when values of eddy viscosity and eddy diffusivity are increased, while keeping the total amount of sediment mass suspended in the water constant. Furthermore, in the case that light attenuation is dominated by suspended sediment in the water, rather than by background turbidity, an increase of water depth enhances the growth of phytoplankton, because the available sediment is distributed over a larger domain.

The present model is not designed to be validated against field data. In particular, including tides and using more sophisticated formulations for eddy viscosity and eddy diffusion coefficients are necessary to make this step. Despite these drawbacks the strength of the model is its transparency and the insight it provides into understanding basic characteristics of phytoplankton dynamics in relation to external forcing conditions.

Acknowledgements

We thank Arjen Doelman and Antonius Zagaris (both at the Centre for Mathematics and Computer Science, Amsterdam, the Netherlands) for many discussions about the contents of this paper. We also thank two anonymous referees for their constructive comments on an earlier version of this paper. The work has been conducted in the framework of the LOICZ project 014.27.013 (Land Ocean Interaction in the Coastal Zone) and administered by NWO-ALW, Netherlands Organization of Scientific Research.

Appendix A. Analytical solution of the eigenvalue problem

Consider the eigenvalue problem (17a) for $\mu = \bar{\mu}$ is constant. This equation allows for exponential solutions $\hat{P} \sim e^{\alpha z}$. Substitution yields a quartic in α, which has solutions $\alpha_\pm$. So the general solution of the equation reads

$$\hat{P} = Ae^{\alpha_+ z} + Be^{\alpha_- z}, \quad \alpha_\pm = \frac{-v \pm (v^2 - 4K_v r)^{1/2}}{2K_v},$$
$$r = \bar{\mu} - m - \lambda. \tag{A.1}$$

The no-flux boundary conditions at surface $z = 0$ and bottom $z = -h$ yield two homogeneous equations for the constants A and B. Imposing the condition of non-trivial solutions results in

$$(K_v\alpha_+ + v)(K_v\alpha_- + v)(e^{\alpha_- h} - e^{\alpha_+ h}) = 0. \tag{A.2}$$

As $(K_v\alpha_+ + v)$ is always positive this equation has two roots.

(1) $K_v\alpha_- + v = 0$.

This yields $r = 0$; hence, $\alpha_+ = 0$ and $\lambda_1 = \bar{\mu} - m$. Substitution in Eq. (17a) shows that the equation for the eigenmode $\hat{P}_1$ becomes

$$\frac{\partial}{\partial z}\left(K_v \frac{\partial \hat{P}_1}{\partial z} + v\hat{P}_1\right) = 0. \tag{A.3}$$

Note that the terms between brackets denote the spatial pattern of the vertical component of the flux of phytoplankton. Using the boundary conditions it follows that the solution of this equation reads

$$\hat{P}_1 = A \exp(-Pe\, z/h), \tag{A.4}$$

with Pe the Péclet number defined in Eq. (18).

(2) $e^{\alpha_- h} - e^{\alpha_+ h} = 0$.

This condition yields the solutions

$$(\alpha_+ - \alpha_-)h = 2\pi i \quad \text{so } r = \frac{v^2 + 4n^2\pi^2 K_v^2/h^2}{4K_v}. \tag{A.5}$$

Using the definition of parameter r (see Eq. (A.1)) and that of the Péclet number it follows that

$$\lambda_{n+1} = \bar{\mu} - m - \frac{v}{4h}\frac{1}{Pe}\left(Pe^2 + 4n^2\pi^2\right), \quad n = 1, 2, \ldots . \tag{A.6}$$

Note that $\lambda_n \to -\infty$ for both $Pe \to 0$ and $Pe \to \infty$. Straightforward algebra shows that mode n can have a positive growth rate if $\bar{\mu} > m + n\pi h/v$.

References

Burchard, H., Baumert, H., 1998. The formation of estuarine turbidity maxima due to density effects in the salt wedge. A hydrodynamic process study. Journal of Physical Oceanography 28, 309–321.

Cloern, J.E., 1991. Tidal stirring and phytoplankton bloom dynamics in an estuary. Journal of Marine Research 49, 203–221.

Festa, J.F., Hansen, D.V., 1978. Turbidity maxima in partially stratified estuaria. Estuarine and Coastal Marine Science 7, 347–359.

Friedrichs, C.T., Armbrust, B.D., De Swart, H.E., 1998. Hydrodynamics and equilibrium sediment dynamics of shallow, funnel-shaped tidal estuaries. In: Dronkers, J., Scheffers, M.B.A.M. (Eds.), Physics of Estuaries and Coastal Seas. PECS 1996. Balkema, Rotterdam, pp. 337–343.

Hansen, D.V., Rattray, M., 1965. Gravitational circulation in straits and estuaries. Journal of Marine Research 23, 104–122.

Helder, W., Ruardij, P., 1982. A one-dimensional mixing and flushing model of the Ems-Dollard estuary: calculation of time scales at different river discharges. Netherlands Journal of Sea Research 15, 293–312.

Huisman, J., Thi, N.N.P., Karl, D.M., Sommeijer, B., 2006. Reduced mixing generates oscillations and chaos in the oceanic deep chlorophyll maximum. Nature 439, 322–326.

Jay, D.A., Musiak, J.D., 1994. Particle trapping in estuarine tidal flows. Journal of Geophysical Research 99 (C10), 445–461.

Lerczak, J.A., Geyer, W.R., 2004. Modeling the lateral circulation in straight, stratified estuaries. Journal of Physical Oceanography 34, 1410–1428.

Li, C., O'Donnell, J., 1997. Tidally driven residual circulation in shallow estuaries with lateral depth variation. Journal of Geophysical Research 102 (C13), 27915–27929.

Lucas, L.V., Cloern, J.E., Koseff, J.R., Monismith, S.G., Thompson, J.K., 1998. Does the Sverdrup critical depth model explain bloom dynamics in estuaries? Journal of Marine Research 56, 375–415.

Lucas, L.V., Koseff, J.R., Cloern, J.E., Monismith, S.G., Thompson, J.K., 1999. Processes governing phytoplankton blooms in estuaries. II. The role of horizontal transport. Marine Ecology Progress Series 187, 17–30.

May, C.L., Koseff, J., Lucas, L.V., Cloern, J.E., Schoellhamer, D.H., 2003. Effects of spatial and temporal variability of turbidity on phytoplankton blooms. Marine Ecology Progress Series 254, 111–128.

Monismith, S.G., Kimmerer, W., Burau, J.R., Stacey, M.T., 2002. Structure and flow-induced variability of the subtidal salinity field in Northern San Fransisco Bay. Journal of Physical Oceanography 32, 3003–3019.

Officer, C., 1976. Physical Oceanography of Estuaries (and Associated Coastal Waters). Wiley, New York.

Postma, H., 1954. Hydrography of the Dutch Wadden Sea. Archives Neerlandaises de Zoologie (Archino Oceanografia Limnologia) 10, 405–511.

Schuttelaars, H.M., De Swart, H.E., 2000. Multiple morphodynamic equilibria in tidal embayments. Journal of Geophysical Research 105 (C10), 24105–24118.

Sin, Y., Wetzel, R.L., Anderson, I.C., 1999. Spatial and temporal characteristics of nutrient and phytoplankton dynamics in the York River estuary, Virginia: analyses of long-term data. Estuaries 22 (2A), 260–275.

Sverdrup, H.U., 1953. On conditions for the vernal blooming of phytoplankton. Journal du Conseil International pour l'Exploration de la Mer 18, 287–295.

Talke, S.A., de Swart, H.E., Schuttelaars, H.M., 2007. Feedback between residual circulations and sediment distribution in highly turbid estuaries: an analytical model. Continental Shelf Research, this issue, doi:10.1016/j.csr.2007.09.002.

Tolhurst, T.J., Defew, E.C., de Brouwer, J.F.C., Wolfstein, J.C., Stal, L.J., Paterson, D.M., 2006. Small-scale temporal and spatial variability in the erosion threshold and properties of cohesive intertidal sediments. Continental Shelf Research 26, 351–362.

Widdows, J., Brown, S., Brinsley, M., Salkeld, P., Elliott, M., 2000. Temporal changes in intertidal sediment erodability: influence of biological and climatic factors. Continental Shelf Research 20, 1275–1289.

Winterwerp, J.C., 2002. On the flocculation and settling velocity of estuarine mud. Continental Shelf Research 22 (9), 1339–1360.

Zagaris, A., Doelman, A., Pham Thi, N.N., Sommeijer, B.P., 2007. Blooming in a non-local, coupled phytoplankton-nutrient model. Submitted to SIAM Journal on Applied Mathematics. Preprint available from:⟨http://www.cwi.nl/doelman/HP_PUB/ZDPS.pdf⟩.

Zimmerman, J.T.F., 1986. The tidal whirlpool: a review of horizontal dispersion by tidal and residual velocities. Netherlands Journal of Sea Research 20, 133–154.